Optics
2018; 7(1): 7-12
http://www.sciencepublishinggroup.com/j/optics
doi: 10.11648/j.optics.20180701.12
ISSN: 2328-7780 (Print); ISSN: 2328-7810 (Online)

Hydrothermal Synthesis of $Tb_2(WO_4)_3$: Eu^{3+} Phosphors with Controllable Morphology and Multicolor Tunable Luminescence

Li Yuan*, Jianwang He, Zhulang Qiu

School of Chemistry and Chemical Engineering, Southwest University, Chongqing, China

Email address:

1208157548@qq.com (Li Yuan)

*Corresponding author

To cite this article:

Li Yuan, Jianwang He, Zhulang Qiu. Hydrothermal Synthesis of $Tb_2(WO_4)_3$: Eu^{3+} Phosphors with Controllable Morphology and Multicolor Tunable Luminescence. *Optics*. Vol. 7, No. 1, 2018, pp. 7-12. doi: 10.11648/j.optics.20180701.12

Received: December 6, 2017; **Accepted**: December 18, 2017; **Published**: January 18, 2018

Abstract: Rare earth doped luminescent materials can be used in fluorescent lamps, display devices, biology and many other fields. Especially, phosphors with controllable morphology and multicolor tunable luminescence have many virtues. Thus, the synthesis of suitable phosphors is very important. Among all the synthesis methods, hydrothermal method stands out. Europium activated terbium tungstate ($Tb_2(WO_4)_3$: Eu^{3+}) phosphors with controllable morphology have been successfully synthesized by hydrothermal method, followed by a subsequent calcination process. X-ray diffraction (XRD), scanning electron microscopy (SEM) and photoluminescence (PL) are employed to characterize the samples. Controlling the reaction parameters, a variety of morphology have been obtained. Thanks to the efficient energy transfer from WO_4^{2-} to Tb^{3+} to Eu^{3+}, $Tb_2(WO_4)_3$: Eu^{3+} phosphors demonstrate outstanding luminescent properties with tunable colors under ultraviolet (UV) excitation, which makes it possible that the emission colors of $Tb_2(WO_4)_3$: Eu^{3+} phosphors can be altered from green, yellow, orange to red with the doped Eu^{3+} content increasing. The facile preparation route and multicolor tunable luminescence make the materials promising candidate phosphors applied in future color displays and light-emitting devices.

Keywords: Hydrothermal Synthesis, Controllable Morphology, Tb^{3+}→Eu^{3+} Energy Transfer, Multicolor Tunable Luminescence

1. Introduction

Rare earth (RE) elements, namely yttrium, scandium and the 14 elements of the lanthanide (Ln) series, are often referred to as the “industrial secret ingredients” due to their unique physical and chemical properties associated with the activities of their f-shell electrons. [1] Currently, RE elements can be involved in practically all everyday activities of modern society because of their enormously wide range of applications, which comprise materials for catalysis, magnets, phosphors, ceramics, polishing, glasses, batteries, among others. [2] Light and rare earths have a long lived relationship that dates from the discoveries of these elements in the nineteenth century. [2] A long lifetime, high mono-chromaticity, a large stokes shift, sharp fluorescence and high resistance to photobleaching make RE-based luminescent materials superior to traditional luminescent materials. [3] Generally speaking, RE-doped luminescent materials can be divided into up-conversion (UC) luminescent materials, and down-conversion (DC) luminescent materials. UC describes the nonlinear process in which a UC material can generate one high-energy photon for every two or more low-energy photons, while for the DC process, it is demonstrated that RE-ion-doped phosphors are able to take up one high-energy incident photon and efficiently convert it into two or more low-energy photons. [4] UC materials are mainly applied in biological field and DC materials are mainly applied in plasma panel displays (PDPs), field emission displays (FEDs), cathode ray tubes (CRTs) and light-emitting diodes (LEDs). [3] LEDs are recognized as

next-generation illumination sources owing to their eco-friendly nature, high-tech design, and promising applications in diverse industries. [5] Nevertheless, commercially used LEDs (blue light chip add yttrium aluminum garnet (YAG) yellow phosphor powder) suffer from low thermal stability and chroma, which significantly influence lighting efficiency and color performance. [5] That is why new phosphors are needed.

Tungstate, as a transition metal salt, is a kind of important phosphor matrix. It is commonly used as scintillating material, optical fiber and magnetic device, and its typical representatives are MWO_4 (M = Mg, Ca, Zn, Pb). To date, a large amount of tungatate nano/micro-crystals have been reported. [6] For example, AWO_4 (A=Ca, Sr, Ba) nanorods have been synthesized using a modified template directed methodology. [7] Tungstates are regarded as prospective host materials for doped RE ions because these RE ions are doped into the tungstate lattice, which makes them have special properties of luminescence. However, the luminescent properties of rare earth tungstate ($RE_2(WO_4)_3$) get much less notice compared with their impressive negative thermal expansion and trivalent cation conducting performances. [8] As a consequence, the exploration of novel $RE_2(WO_4)_3$ materials with splendid luminescent properties draws an increasing attention.

Rare-earth ions have been occupying an irreplaceable position in modern lighting and display fields due to the abundant emission colors based on their 4f→4f or 5d→4f transitions. [5] Energy transfer between RE ions should not be ignored in the color tuning of single-phase phosphors from the theoretical and practical points of view. Many RE ions peculiarly Eu^{3+} and Tb^{3+} ions have been widely investigated by researchers because of their outstanding down-conversion luminescent properties. [3] The energy transfer from Tb^{3+} to Eu^{3+} in some hosts has already been reported in many researches. I. Koseva et al. reported $NaAlSiO_4$ glass-ceramics co-doped by Tb^{3+} and Eu^{3+} ions, [9] from which we can see that Tb^{3+} and Eu^{3+} ions are all co-doped in a third-party hosts, and that means multicolor emissions can only be implemented by co-doping at least two rare earth ions, complicating the synthesis route and energy transfer process. Until now, only a few reports about the Tb^{3+}→Eu^{3+} energy transfer have been connected with Eu^{3+}-doped terbium-based hosts. [10] Herein, we have successfully synthesized $Tb_2(WO_4)_3$: Eu^{3+} phosphors, in which energy transfer can take place not just from Tb^{3+} to Eu^{3+} but also from WO_4^{2-} to Tb^{3+} out of WO_4^{2-}→Tb^{3+} energy transfer under the ultraviolet excitation. That is to say, by simply adjusting the doped Eu^{3+} content, multicolor emissions (from green, yellow, orange to red) can be achieved in a single host material ($Tb_2(WO_4)_3$).

As we all know, well-dispersed and uniform morphology contribute to phosphors' chemical stability as well as their luminescent properties. Among all the preparation methods, the hydrothermal method is one of the most efficient way to synthesize materials with uniform and controllable morphology. [11]

In this report, we take advantage of the efficiency of hydrothermal method and successfully synthesize $Tb_2(WO_4)_3$: Eu^{3+} phosphors with controllable morphology and multicolor luminescent properties. Influences of different experimental conditions, namely surfactant and pH values, on the precursors' morphology are investigated in detail in order to find the optimal experimental condition. What is more, multicolor emissions (from green, yellow, orange to red) are achieved in a single host material ($Tb_2(WO_4)_3$) by simply adjusting the doped Eu^{3+} content.

2. Experimental Section

2.1. Materials

All starting materials in the present work were of analytical grade and used without further purification. Europium oxide (Eu_2O_3, 99.99%), terbium oxide (Tb_4O_7, 99.99%), hydrogen nitrate (HNO_3), sodium hydroxide (NaOH), sodium tungstate dihydrate ($Na_2WO_4{\cdot}2H_2O$), polyvinyl pyrrolidone (PVP), glycine (Gly), cetyltrimethyl ammonium bromide (CTAB), sodium dodecyl benzene sulfonate (SDBS), ethylene diamine tetraacetic acid (EDTA), were purchased from Aladdin Industrial Corporation (China). $Tb(NO_3)_3$ and $Eu(NO_3)_3$ were prepared by dissolving Tb_4O_7 and Eu_2O_3 in hot dilute HNO_3 solution followed by the evaporation of excess HNO_3.

2.2. Preparation

In a typical synthesis process, surfactant and 35ml of deionized water were mixed in a 100 ml beaker under strong magnetic stirring at room temperature for 10 minutes until 1mmol $Tb(NO_3)_3$ solution ($1mol{\cdot}L^{-1}$) and appropriate amounts of $Eu(NO_3)_3$ solution were added into it. After another 20-minute vigorous stirring, 0.4948g $Na_2WO_4{\cdot}2H_2O$ was added into the above solution, and the pH value of the mixture was adjusted to 4 by NaOH before an additional 30-mintue agitation. Then, the obtained solution was transferred to a 50 ml Teflon-lined autoclave (filled up to 80% of its total volume), which was sealed and maintained at 200°C for 24 h. After the autoclave cooling to room temperature naturally, the precipitates were collected by centrifugation, washed with deionized water and ethanol twice each, and then dried at 80°C for 12 h. Finally, the as-obtained precursors were subjected to further calcination at 800°C for 4 h to form the final products.

2.3. Characterization

All measurements were carried out at room temperature. Powder X-ray diffraction (XRD) was performed on a Purkinje General Instrument MSAL-XD3 using Cu Ka radiation (l = 0.15406nm). Morphology of various materials was characterized using a field emission scanning electron microscopy system (Hitachi S-4800) with an acceleration voltage of 10kV. The photoluminescence (PL) measurements were performed on a Hitachi F-7000 spectrophotometer (a 150 W xenon lamp as the excitation source).

3. Results and Discussion

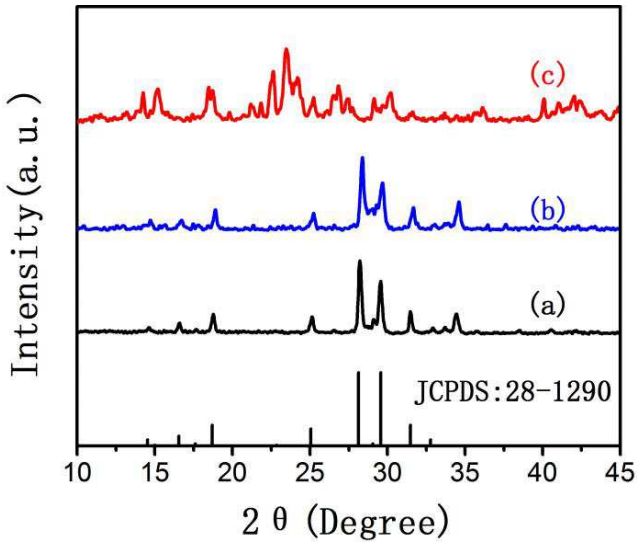

Figure 1. *XRD patterns of (a) $Tb_2(WO_4)_3$, (b) $Tb_2(WO_4)_3$: 1%Eu^{3+}, (c) $Tb_2(WO_4)_3$ precursors.*

3.1. Crystal Structures and Morphology of Samples

Figure 1 demonstrates the XRD patterns of $Tb_2(WO_4)_3$ under diverse circumstances. In Figure 1a, the XRD pattern of $Tb_2(WO_4)_3$ without doping Eu^{3+} is compatible with the standard JCPDS card (No.28-1290) for $Tb_2(WO_4)_3$. In Figure 1b, the XRD pattern of $Tb_2(WO_4)_3$: 1%Eu^{3+} shows the similar diffraction pattern with $Tb_2(WO_4)_3$. No obvious shifting of peaks or other impurity phase could be detected at the current doping level, indicating that Eu^{3+} ions are completely dissolved in the $Tb_2(WO_4)_3$ host lattice. [12] As is shown in Figure 1c, there is a world difference between $Tb_2(WO_4)_3$ precursors and standard JCPDS card (No.28-1290), proving that the calcination process matters a lot in the preparation of pure $Tb_2(WO_4)_3$ crystal.

Figure 2 shows the influence of different surfactant on the formation of $Tb_2(WO_4)_3$ crystal. With the assistance of PVP, Gly, CTAB, and SDBS, we can obtain comparatively pure $Tb_2(WO_4)_3$ crystal, while EDTA does no help. Effects of different pH values can easily be seen in Figure 3, which tells us when pH values are 3, 4, and 5, it is beneficial to the purity of $Tb_2(WO_4)_3$ crystal.

It is generally accepted that the micro-morphology (size, shape, dimensionality, distribution, etc.) of phosphors has a profound influence on their luminescence properties. At the same time, a uniform and well-dispersed morphology can greatly improve their properties as well as their stability. [12] As for phosphors, well-dispersed particles with narrow size distribution are essential because they can potentially improve the screen brightness and increase the resolution on account of a lower scattering of evolved light and higher packing density. [3] This is why if we anticipate to achieve materials with outstanding luminescence properties, controllable synthesis of well-dispersed morphology is required.

The SEM images are used to characterize the morphology of as-prepared $Tb_2(WO_4)_3$ samples. Figure 4 illustrates SEM images of $Tb_2(WO_4)_3$ samples with different kinds of surfactant. Although the representative overview morphology of $Tb_2(WO_4)_3$ is approximately composed of microspheres, the detailed morphology varies from different surfactant and pH values. When the surfactant is PVP (Figure 4a), the morphology of the obtained $Tb_2(WO_4)_3$ samples tends to form sphere, but it actually has no specific structure. When it comes to Gly (Figure 4b) and SDBS (Figure 4d), their morphologies have something in common, they are more sphere-like, but still, they are not formed completely. Besides, their both have agglomeration and nonuniformity in size distribution. In contrast, with CTAB as the organic addictive (Figure 4c), the morphology perform a more uniformity in size distribution and less agglomeration. According to this result, it is reasonable to draw the conclusion that CTAB is the most suitable for the morphology of $Tb_2(WO_4)_3$ samples among these four types of organic addictive.

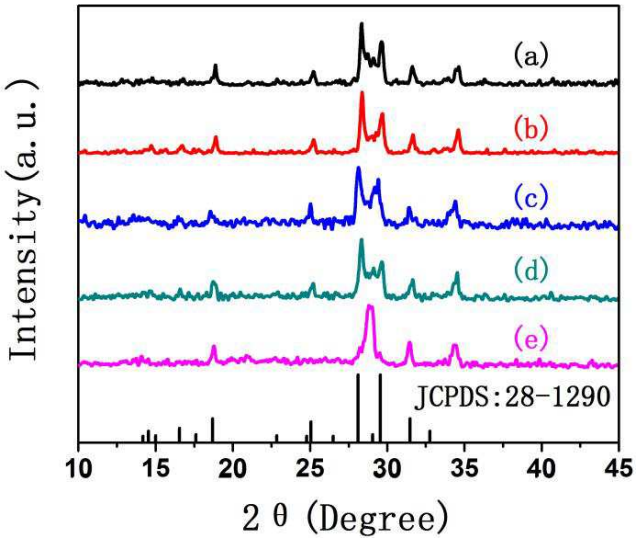

Figure 2. *XRD patterns of $Tb_2(WO_4)_3$ products prepared using different surfactants (a) PVP, (b) Gly, (c) CTAB, (d) SDBS, (e) EDTA.*

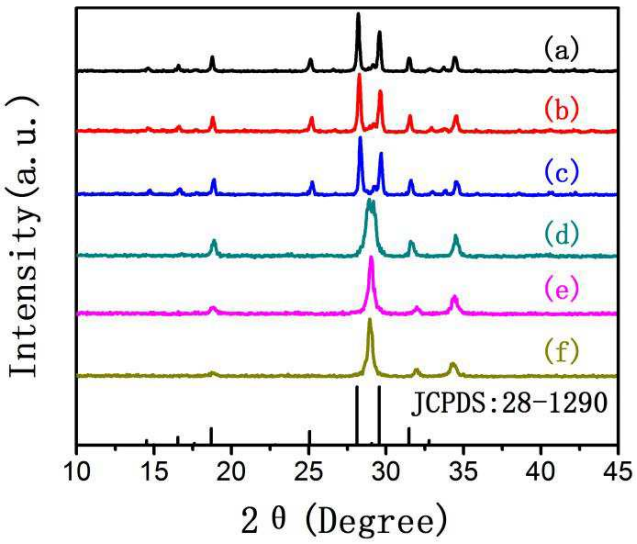

Figure 3. *XRD patterns of $Tb_2(WO_4)_3$ products prepared using CTAB as surfactant at different pH values (a) 3, (b) 4, (c) 5, (d) 6, (e) 7, (f) 8.*

Figure 5 exhibits the SEM images of $Tb_2(WO_4)_3$ samples prepared with the assistance of organic additive CTAB under a series of pH values, where we can see how the morphology of $Tb_2(WO_4)_3$ varies from different pH values. The morphology of $Tb_2(WO_4)_3$ is critically dependent on the pH value during the hydrothermal process. When the experiment is performed at pH =3, adjusting with HNO_3, nanoparticles firstly assemble to form bigger ones, then the bigger ones continue assembling for sphere-like structures with average size of 4 μm in diameter. When the pH value of the solution is 4, we get well-proportioned, well-dispersed and regular microspheres with narrow size distribution as is shown in Figure 5b. The diameter of the particles is in the vicinity of 5μm, which can provide the phosphors a lower scattering of evolved light and higher packing density. Upon a further increase of the pH value up to 5, the particles demonstrate irregularity again. The particles in Figure 5c show similarity in shape with Figure 5a, but are approximately twice the size of that in Figure 5a. When the sample are prepared at pH=6, the precursors show flower-like morphology which aggregates some smooth nanoplates. With the pH value keeping ascending to 7 and 8, the morphology of precursors are composed of numerous irregular nanoplates without any regular structures being detected. According to this experimental result, we find out that the best experimental condition is when pH =5.

3.2. Luminescent Properties of $Tb_2(WO_4)_3$ and $Tb_2(WO_4)_3$: Eu^{3+}

Figure 6a illustrates the excitation spectrum of $Tb_2(WO_4)_3$ by monitoring the emission of Tb^{3+} ($^5D_4 \rightarrow {}^7F_5$) [13] at 549nm. It is made up of an intense broad absorption band with maximum at 275nm in the range of 200–310nm due to the intense charge transfer absorption in WO_4^{2-} group, in which an electron in oxygen (O) 2p orbital transfers into one of the empty tungsten (W) 5d orbits. [14] From 310nm to 500nm in the longer wavelength region, the characteristic f→f transitions within Tb^{3+} $4f^8$ configuration are assigned to the transitions from $^7F_6$ ground state to different excited states of Tb^{3+}. The emission spectrum of $Tb_2(WO_4)_3$ which consists of some sharp f→f transition lines (Figure 6b) appears by exciting WO_4^{2-} group at 275nm. The strongest emission (Tb^{3+}) locates at 549nm in the green region ($^5D_4 \rightarrow {}^7F_5$), whereas the intrinsic emission of WO_4^{2-} groups in the blue region is very weak and almost invisible. The existence of the absorption band of WO_4^{2-} group in the excitation spectrum by monitoring the emission of Tb^{3+} ions ($^5D_4 \rightarrow {}^7F_5$) and the existence of intense emissions of Tb^{3+} ions by exciting the WO_4^{2-} group at 275nm provide the evidence that an efficient energy transfer from WO_4^{2-} to Tb^{3+} occurs.

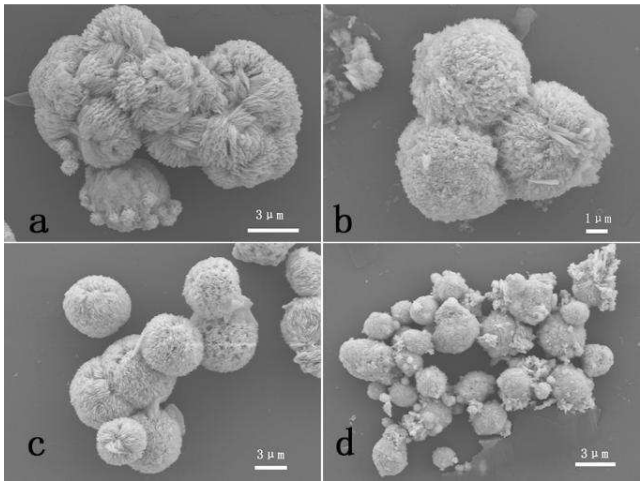

Figure 4. *SEM images of the $Tb_2(WO_4)_3$ products with different surfactant (a) PVP, (b) Gly, (c) CTAB, (d) SDBS.*

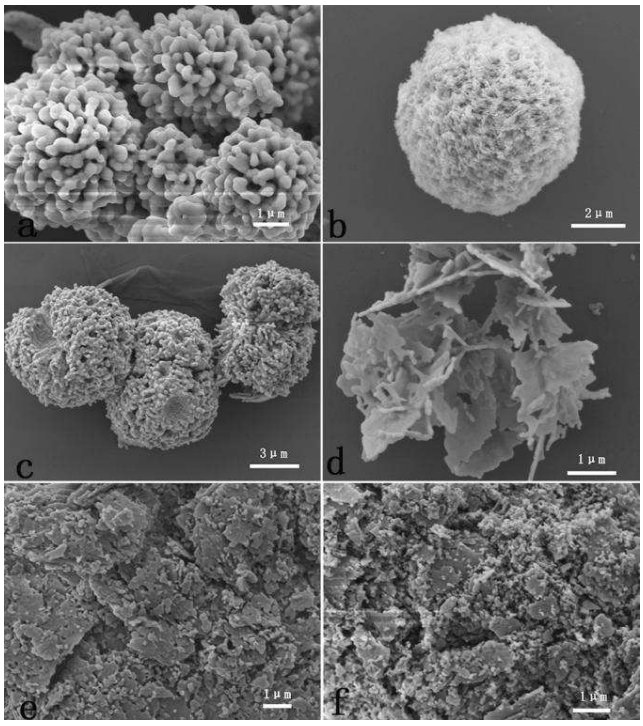

Figure 5. *SEM images of $Tb_2(WO_4)_3$ products prepared using CTAB as surfactant at different pH values (a) 3, (b) 4, (c) 5, (d) 6, (e) 7, (f) 8.*

According to Figure 1, a slight of doped Eu^{3+} ions do not influence the phase of the $Tb_2(WO_4)_3$ host because the XRD pattern still matches well with the standard JCPDS card (No.28-1290) after doping, nevertheless, it has a profound influence on the luminescent property of the host material. After doping Eu^{3+} ions, the luminescent property in Figure 7 changes significantly compared with that in Figure 6. Figure 7a illustrates the excitation spectrum of $Tb_2(WO_4)_3$: 5%Eu^{3+} by monitoring at 619nm ($^5D_0 \rightarrow {}^7F_2$). [13] From 200 to 500nm, there are no obvious differences between Figure 6a and Figure 7a, except for some weak f→f transition lines within the Eu^{3+} $4f^6$ configuration appearing from 380 to 470nm in Figure 7a. Figure 7b presents the emission spectrum of $Tb_2(WO_4)_3$: 5%Eu^{3+} excited at 275nm, in which the

characteristic transitions of Eu^{3+} appear ($^5D_0 \rightarrow {}^7F_1$ 595nm, $^5D_0 \rightarrow {}^7F_2$ 619nm) while transitions of Tb^{3+} ($^5D_4 \rightarrow {}^7F_6$ 491nm, $^5D_4 \rightarrow {}^7F_5$ 549nm) weaken a lot. When monitored at λem =619nm (Eu^{3+}, $^5D_0 \rightarrow {}^7F_2$), except for weak Eu^{3+} characteristic absorption peaks, absorption peaks of WO_4^{2-} and Tb^{3+} ions appear as well in the excitation spectrum. Meanwhile, when excited at λex=275nm (WO_4^{2-}), intense emissions of Eu^{3+} and Tb^{3+} ions appear in the excitation spectrum, from which we can infer that an efficient energy transfer from WO_4^{2-} to Tb^{3+} to Eu^{3+} takes place. Figure 7c presents the emission spectra of $Tb_2(WO_4)_3$: 5%Eu^{3+} upon excitation at 489nm in order to validate the energy transfer from Tb^{3+} to Eu^{3+}. 489nm belongs to the characteristic excitation wavelength of Tb^{3+} ($^7F_6 \rightarrow {}^5D_4$), therefore, when excited at 489nm, the specific intense emission peaks of Tb^{3+} should have shown up by rights, but strong emission of Eu^{3+} appears instead. On the basis of the above analysis, an efficient energy transfer from WO_4^{2-} to Tb^{3+} to Eu^{3+} occurs in $Tb_2(WO_4)_3$: 5% Eu^{3+} phosphor, obviously.

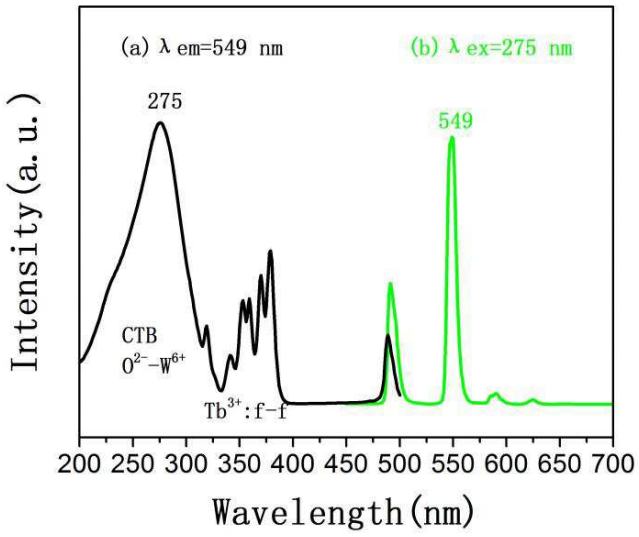

Figure 6. *(a) Excitation and (b) emission spectra of $Tb_2(WO_4)_3$.*

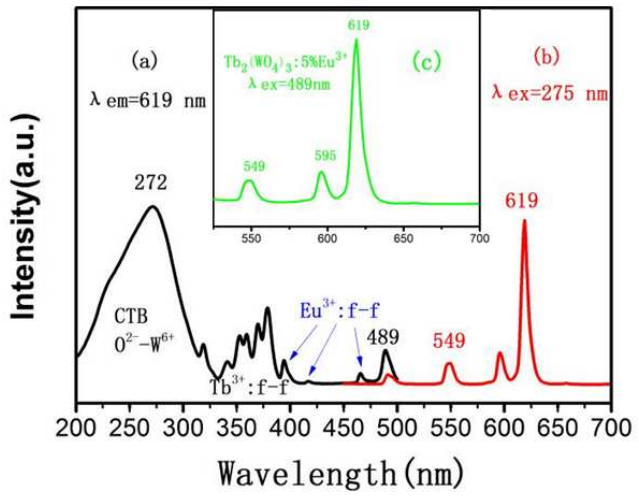

Figure 7. *(a) Excitation and (b) (λex=275nm) (c) (λex=489nm) emission spectra of $Tb_2(WO_4)_3$: 5%Eu^{3+}.*

3.3. CIE Chromaticity

The emission colors of $Tb_2(WO_4)_3$ and $Tb_2(WO_4)_3$: x%Eu^{3+} are analyzed and confirmed on the basis of the corresponding CIE chromaticity coordinates. The CIE chromaticity coordinate for $Tb_2(WO_4)_3$ phosphor is (x=0.2717, y=0.6135) when excited at 275nm. The $Tb_2(WO_4)_3$ phosphor exhibits bright green emission with higher color saturation and monochromaticity, which is superior to the well-known green phosphors (Zn, Cd)S: Ag (0.26, 0.60) and ZnS: $Au_{0.05}$, $Cu_{0.01}$ (0.267, 0.582). [15] The CIE chromaticity coordinates for $Tb_2(WO_4)_3$: 3%Eu^{3+} and $Tb_2(WO_4)_3$: 5%Eu^{3+} are (x=0.4157, y=0.4900) and (x=0.5279, y=0.4148), which belong to yellow and orange region respectively. The CIE chromaticity coordinate for $Tb_2(WO_4)_3$: 35%Eu^{3+} is (x=0.6346, y=0.3232) under excitation at 275nm, which is close to National Television System Committee (NTSC) red phosphor (0.67, 0.33). [16] Altering the Eu^{3+} concentration, CIE coordinates can be tuned from (0.2717, 0.6135) to (0.6346, 0.3232) via (0.4157, 0.4900) and (0.5279, 0.4148), and the corresponding emission colors can be altered from green, yellow, orange to red. That is to say, tunable multicolor emissions can successfully obtained by doping Eu^{3+} in a single host $Tb_2(WO_4)_3$. The most important of all, now that we have got green and yellow emitting phosphors, we may obtain white emitting phosphors by mixing them with proper proportion.

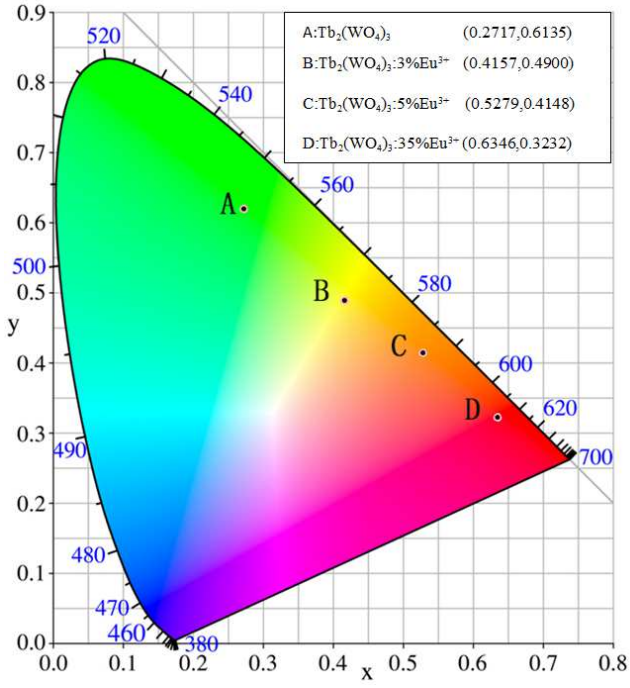

Figure 8. *CIE Chromaticity diagram of $Tb_2(WO_4)_3$: x%Eu^{3+}.*

4. Conclusion

In summary, $Tb_2(WO_4)_3$: Eu^{3+} phosphors have been successfully synthesized by hydrothermal method followed by subsequent calcination treatment. The materials present uniform and well-dispersed microspheres with the average diameter about 5μm. The influences on the formation of

microstructures are systematically investigated. When Eu^{3+} ions are introduced, $Tb_2(WO_4)_3$ can serve as a good host matrix and exhibit strong multicolor PL emissions from green to red resulting from the effective energy transfer from WO_4^{2-} to Tb^{3+} to Eu^{3+}. We anticipate that this hydrothermal method with subsequent calcination can also be extended to the controllable synthesis of other inorganic materials. The obtained green and red phosphors can be potentially applied in many fields such as phosphors, luminescent materials, photo catalysts, etc.

Acknowledgements

This project is financially supported by the National Undergraduate Training Program for Innovation and Entrepreneurship of Southwest University, China (201610635065).

References

[1] D. Xue, H. Zhang, Y. Liu, S. Yin, L. Lu and J. H. Boo, *Mater. Res. Bull.* 2017, *96*, 1.

[2] P. C. d. Sousa Filho, J. F. Lima and O. A. Serra, *J. Brazil. Chem. Soc.* 2015, *26*, 2471.

[3] L. Zhou, L. Yuan, X. Zhou, S. Hu, Y. Hu, Y. Luo and J. Yang, *Chemistry Select* 2016, *1*, 1848.

[4] H.-Q. Wang, M. Batentschuk, A. Osvet, L. Pinna and C. J. Brabec, *Adv. Mater.* 2011, *23*, 2675.

[5] X. Wu, Y. Liang, S. Liu, Y. Zhu, R. Xu, M. Tong and K. Li, *Spectrosc. Lett.* 2017, *50*, 48.

[6] B. Zhao, L. Yuan, S. Hu, X. Zhang, X. Zhou, J. Tang and J. Yang, *Cryst Eng Comm* 2016, *18*, 8044.

[7] F. Zhang, M. Y. Sfeir, J. A. Misewich and S. S. Wong, *Chem. Mater.* 2008, *20*, 5500.

[8] B. A. Marinkovic, P. M. Jardim, R. R. d. Avillez and F. Rizzo, *Solid State Sci.* 2005, *7*, 1377.

[9] I. Koseva, P. Tzvetkov, P. Ivanov, A. Yordanova and V. Nikolov, *Optik* 2017, *137*, 45.

[10] Y. Zhang, W. T. Gong, J. J. Yu, Z. Y. Cheng and G. L. Ning, *RSC Adv.* 2016, *6*, 30886.

[11] Y. Tian, B. J. Chen, B. N. Tian, J. S. S. N. S. Yu, X. P. Li, J. S. Zhang, L. H. Cheng, H. Y. Zhong, Q. Y. Meng and R. N. Hua, *J. Colloid Interf. Sci.* 2013, *393*, 66.

[12] J. Yang, L. Zhou, L. Yuan, X. Zhou, B. Hu, X. Zhang and S. Hu, *New J. Chem.* 2016, *40*, 7350.

[13] J. Yang, C. Li, Z. Quan, C. Zhang, P. Yang, Y. Li, C. Yu and J. Lin, *The Journal of Physical Chemistry C* 2008, *112*, 12777.

[14] Z. Y. Hou, Z. Y. Chen, G. G. Li, W. X. Wang, C. Peng, C. X. Li, P. A. Ma, D. M. Yang, X. J. Kang and J. Lin, *Nanoscale* 2011, *3*, 1568.

[15] J. Wang, Y. H. Xu and M. Hojamberdiev, *J. Alloys. Compd.* 2009, *481*, 896.

[16] S. Cao, Y. Jiao, W. Han, C. Ge, B. Song, J. Wang and X. Zhang, *Spectrochim. Acta A* 2018, *190*, 231.